Direct density measurement of shock-compressed iron using hard x rays generated by a short laser pulse

E. Brambrink,[1,*] H. G. Wei,[1,2,3] B. Barbrel,[1,4] P. Audebert,[1] A. Benuzzi-Mounaix,[1] T. Boehly,[5] T. Endo,[6] C. D. Gregory,[1] T. Kimura,[6] R. Kodama,[6] N. Ozaki,[6] H.-S. Park,[7] and M. Koenig[1]

[1]*LULI, Ecole Polytechnique, CEA, UPMC Université Paris 06, 91128 Palaiseau, France*

[2]*Shandong University, Jinan, 250100, China*

[3]*National Astronomical Observatories, Chinese Academy of Science, Beijing, 100012, China*

[4]*Département de Physique Théorique et Appliquée, CEA/DAM, Bruyères-le-Châtel, 91297, Arpajon, France*

[5]*Laboratory for Laser Energetics, University of Rochester, Rochester, New York, 14623 USA*

[6]*Graduate School of Engineering, Osaka University, Suita, Osaka 565-0871, Japan*

[7]*Lawrence Livermore National Laboratory, Livermore, California 94551-0808, USA*

(Received 26 August 2009; published 24 November 2009)

We present the application of short-pulse laser-driven hard x rays (>40 keV) for the direct density measurement of iron compressed by a laser-driven shock. By using an on-shot calibration of the spectral absorption, we are able to obtain line densities with 5%–10% precision, although the x-ray source is not monochromatic. We also discuss possibilities for increasing the precision, which would be an improvement for equation of state measurements.

DOI: 10.1103/PhysRevE.80.056407 PACS number(s): 52.38.Ph

I. INTRODUCTION

The equation of state (EOS) of materials in the high-pressure and high-density domain is still under investigation due to controversy surrounding theoretical modeling and its importance for other fields. Models in astrophysics [1], planetary physics, geophysics [2], and inertial confinement fusion [3,4] depend strongly on correct EOS. Therefore improving the precision of EOS measurements is an important input for these fields.

Laser-driven shocks are now one of the standard methods used to create high-pressure states of matter in the multiple Mbar range [5]. The determination of the EOS requires the independent measurement of two parameters, shock velocity, and particle velocity for example.

Presently, measurements of EOS are mainly based on the measurement of the shock velocity (e.g., in transparent media) and the free-surface velocity or the interface velocity between the shocked sample and a release window, deducing pressure and density with the Rankine-Hugoniot relations. Measuring an additional parameter such as the density is useful for validating the measurements and increasing precision. X-ray radiography is one possibility for performing a direct density measurement. Typical sample sizes of >500 μm used for EOS measurements with lasers require high photon energies (>50 keV) to probe mid-Z material.

A high-quality radiograph requires an x-ray source with good spatial ($\approx$10 μm) and temporal resolution (<100 ps) to resolve the shock front. In addition, a good dynamic resolution of the detector is needed to precisely determine the density. Short-pulse laser-driven x-ray sources are an excellent candidate, as they can deliver high-energy photons in short bursts [6]. The spatial resolution can be achieved by using small targets, thus providing a point source [7,8].

Such a technique has already been demonstrated for shocked aluminum [9] using 17.5 keV x rays. We have applied this method to radiograph iron using 60 keV x-ray photons from a W target to match the shorter x-ray absorption length of iron. 60 keV photons have 62% transmission through a 500 μm thick iron sample, thus providing well measurable changes for a compression of 1.5–2. Tungsten is also stable and easily available in various shapes and sizes down to a few μm. In addition, we used an x-ray source providing a good spatial resolution in two dimensions and introduced an on-shot density calibration, which improved the precision of the density measurement.

II. EXPERIMENTAL SETUP

The experiments were performed at the LULI 2000 laser system, employing a setup as show in Fig. 1. We used a long-pulse beam with 400 J in 1.5 ns at 527 nm to launch the shock. Hybrid phase plates (HPPs) were used to provide a 400 μm diameter focal spot, containing 30% of the laser

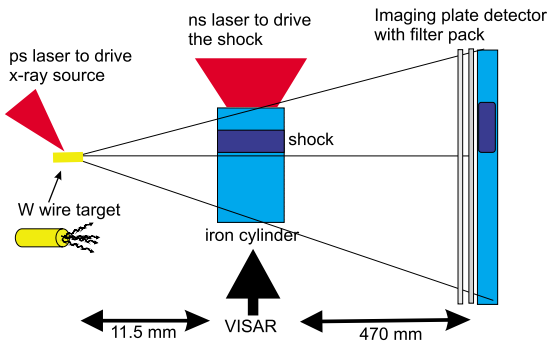

FIG. 1. (Color online) Schematics of the experimental setup (not drawn to scale). The long pulse drives a shock (illustrated by a dark slice in the cylinder) into a small iron cylinder while the short-pulse laser is used to drive the x-ray source.

*erik.brambrink@polytechnique.edu

energy on target. The focal spot has a flat-top profile with intensity modulations due to speckles of 30%–50%. However, these speckles are too small to alter the flatness of the shock front. The flatness of the shock break-out measured on thin targets confirms this.

The x-ray source was driven by a hybrid CPA laser system delivering sub-ps pulses up to 40 J at 1057 nm wavelength. For this experiment the pulse was stretched to 10 ps length by detuning the compressor. The focused intensity was 2×10^{18} W/cm^2. Both amplified spontaneous emission (ASE) and prepulse level were not characterized due to a diagnostic failure during the experiment. Measurements after the experiment indicate an ASE intensity level of $>10^{-4}$ (relative to the 10 ps pulse) over 3 ns. We observed also discrete prepulses of 10^{-2} 100 ps before the main pulse.

The axis of short- and long-pulse laser arrives with an angle of 112.5° to each other in the target chamber. The jitter between the two pulses is better than 30 ps.

The shocked target was an iron cylinder of 500 μm diameter and 250 μm thickness. This cylinder was glued onto an 10 μm thick iron foil with a 15 μm thick plastic coating which served as an ablator. The x-ray source targets were free-standing W wires of 18 μm diameter, pointing toward the iron cylinder, thus providing a two-dimensional resolution x-ray radiography [8]. The distance between the two targets was 11.5 mm.

The radiography was recorded with an imaging plate (IP) [10]. IPs are coated with small grain BaFBrI:Eu2+ crystals, which can be excited into a metastable atomic level. In the scanner the plate is irradiated with a laser, which stimulates the de-excitation of the metastable atoms. A photomultiplier tube then detects the photons. The scanner gives a value, which is proportional to the number of photostimulated luminescence photons (PSLs). This PSL value is proportional to the x-ray yield, but the proportionality factor depends on the photon energy.

The IP was placed at a distance of 47 cm from the iron cylinder, providing a magnification of 42. The detector was covered by 12 mm plastic and 2 mm Al to block particles and low-energy x rays. We also placed a Fe step target in front of the filter to obtain the dynamic detector response (see below).

In order to have an independent characterization of the shock, the rear surface velocity was measured with a velocity interferometer system for any reflector (VISAR) [11]. With this diagnostic the arrival time of the shock at the end of the cylinder can be measured precisely.

III. RADIOGRAPHY RESULTS

After recording an x-ray radiograph, the imaging plate was digitized with a BAS-5000 reader. A radiograph of a shocked iron cylinder is shown in Fig. 2. We observed a very low x-ray flux in this experiment compared to extrapolation from previous studies, which decreases the signal-to-noise ratio (SNR) (see [8]).

As we have chosen a very high magnification, the resolution per pixel (1 μm per pixel in the object plane) is much higher than the resolution given by the source size (18 μm).

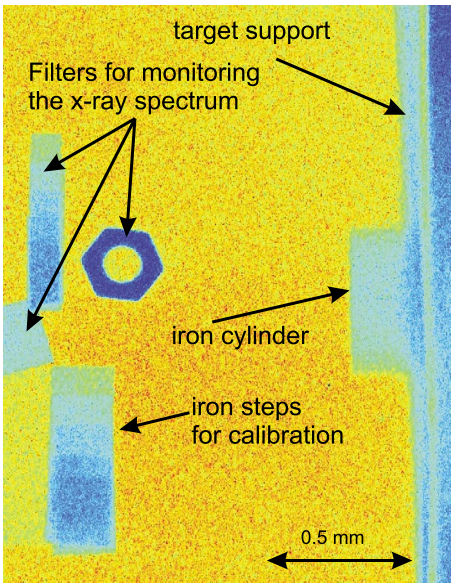

FIG. 2. (Color online) Digitized image of the radiograph showing the shocked target with support and the step wedge for calibration 8 ns after the onset of the long-pulse laser. The filters for monitoring the x-ray spectrum are not discussed in this article. The axis of the iron cylinder is horizontal in this image

Therefore we can smooth the image without losing information. After smoothing over 12 pixels in both dimensions we obtain the radiograph shown in Fig. 3. The shock front is clearly visible as well as the gradual decrease in the transmission toward the center of the cylinder. A lineout through the cylinder was taken (marked with a line in Fig. 3) to obtain the profile of the transmitted x-ray signal.

The difference between shocked and unshocked regions also appears in the transmission profiles through these regions as shown in Fig. 4. Although the transmission is noisy, we observe a significant difference. For a quantitative analysis, it is necessary to transform the transmission to line densities, which can then be treated with an Abel inversion.

In contrast to monochromatic sources, the calculation from transmission to line density is not straight forward, as

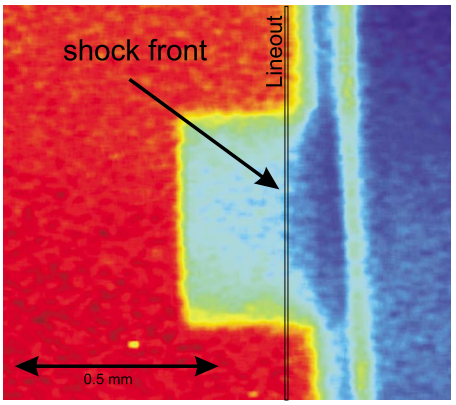

FIG. 3. (Color online) Iron cylinder with shock front after smoothing of the image. The shock propagating into the target is clearly visible. The edge function of cylinder corresponds to 20 μm spatial resolution.

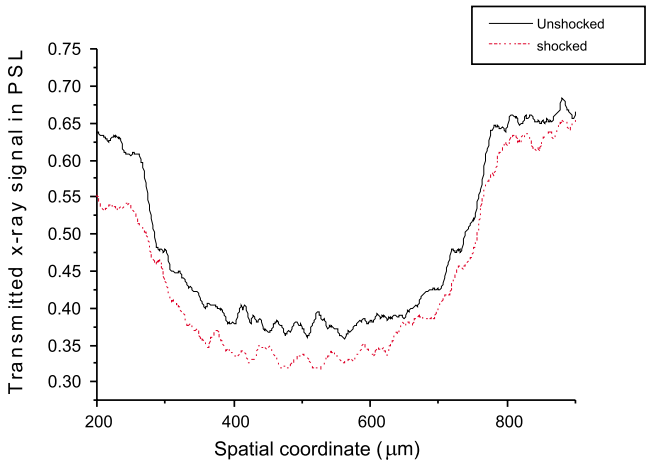

FIG. 4. (Color online) Transmission profile through shocked and unshocked regions. The transmission changes significantly in the shocked region

the spectrum cannot be measured completely; thus the transmission of the different spectral components cannot be calculated [12]. Therefore we have chosen an on-shot calibration with a step target from 0 to 1 mm iron in 200 μm steps. This gives a direct correlation between the measured x-ray signal (PSL) and the line density. This correlation is shown in Fig. 5.

This on-shot calibration has been tested with the unshocked region of the cylinder, where the line density is known. Figure 6 shows calculated x-ray intensities on the detector for different cylinder diameters compared to the measured signal. Despite the noise, a difference of 5% is clearly visible, deviations of the measured line density from the theoretical one are within 8%. Thus the on-shot calibration is a precise method.

With this calibration we then calculated the line density for the shocked and unshocked regions. The result is shown in Fig. 7. The line density in the center is approximately 30% higher than that for the unshocked case. Compared to the

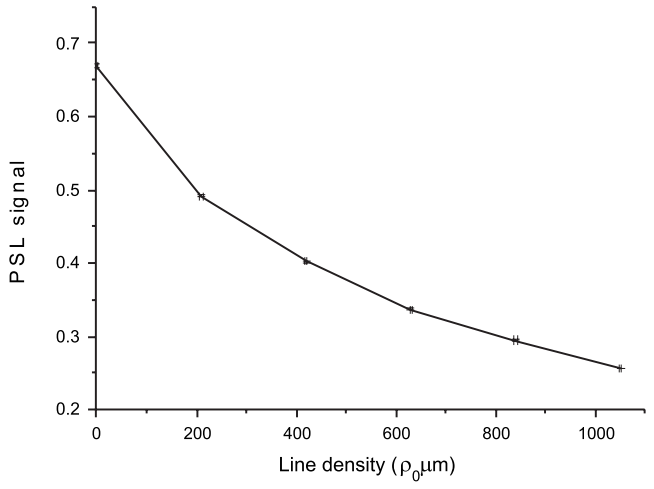

FIG. 5. On-shot calibration of the x-ray transmission for several line densities. Averaging over the relatively large size of the step wedge results in very small error bars for the x-ray signal.

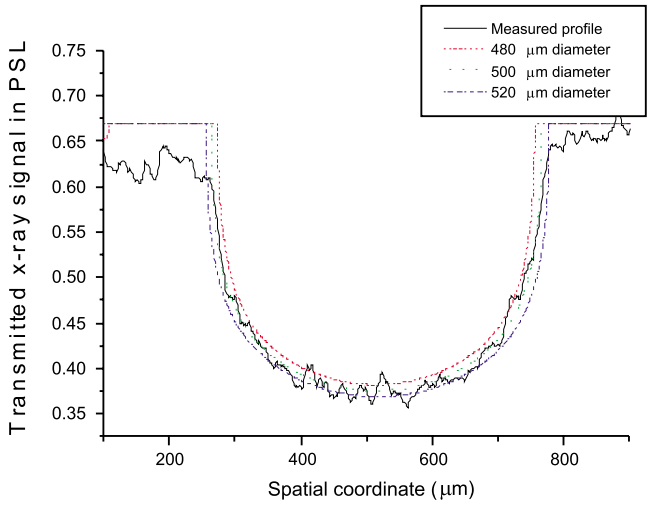

FIG. 6. (Color online) Calculation of the transmitted x-ray signal for different iron cylinder diameters. Even the relatively noisy data allow a line-density measurement better than 8%.

error in line density of 8%, the line density increase is significant. The graph also contains different fit functions for the line density, as the data itself is too noisy to be used directly for the Abel inversion, which provides a radial density profile. Comparing the results of these different functions allows an estimate of the error occurring in the Abel inversion due to the error in the line-density measurement.

Figure 8 shows the radial profile for the different fits of the line density. The maximum compression on the cylinder axis varies between 1.4 and 1.6. So the choice of the fit function alone introduces an error of more than 10%. Taking into account the possible error in the line-density profile of 5%–10%, the total error of the compression is $\pm$20–30%.

IV. DISCUSSION

In order to gain a better understanding of the results, we performed one-dimensional simulations using MULTI [13], a

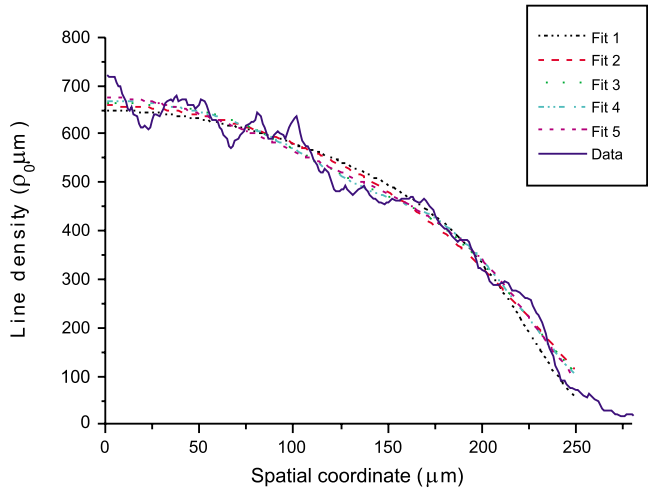

FIG. 7. (Color online) Extracted line-density for the shocked region with the on-shot calibration and a set of fit curves, which are used for the Abel inversion afterwards. This set of line-density fits allow an estimate of the error of the Abel inversion.

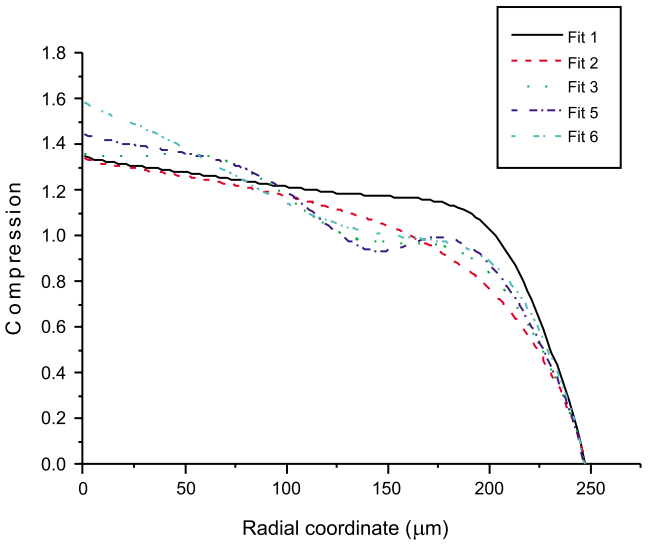

FIG. 8. (Color online) Radial density profile calculated from line-density using Abel inversion. The maximum compression in the center is ≈1.4–1.5.

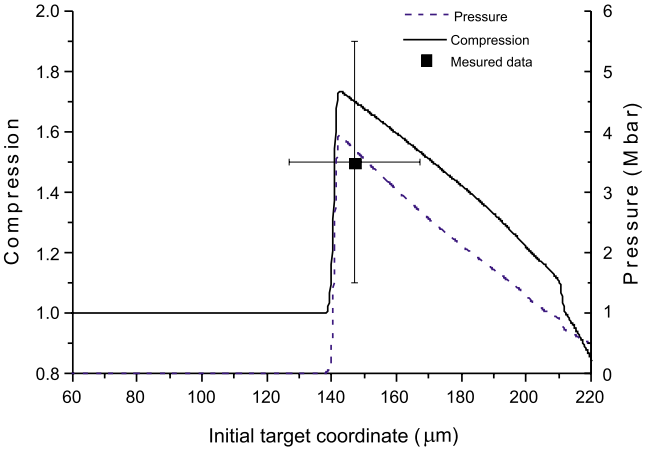

FIG. 9. (Color online) Compression and pressure profiles along the cylinder axis after 8 ns obtained with hydrodynamic simulations. The measured compression is lower than that obtained from the simulation, but within the error bars. Also, the position of the shock front is well reproduced

radiative hydrodynamic code. The equation of states was taken from the SESAME Tables [14]. The simulations reproduced the correct shock breakout time at the rear side of the cylinder, which was measured with the VISAR. Note that the x axis is along the cylinder axis (perpendicular to the line out of Fig. 4) and positions are given as mass coordinates (Lagrangian coordinates).

Figure 9 shows the compression and pressure profiles after 8 ns, which corresponds to the time when the radiograph was taken. The maximum compression of 1.7 is 10%–20% higher than the result obtained with the radiography, but still within the limits of the method with the present SNR of the x-ray signal. The position of the shock front is consistent within the error bars with the values obtained from the radiography.

The density measurement performed in the described experiments is lacking the necessary precision to discriminate between different theoretical models. This is due to the relatively low x-ray flux, introducing strong statistical noise during detector readout. Raising the photon flux will decrease the SNR by a factor 5 or more.

The comparably low x-ray flux observed in this experiment is probably related to a large prepulse, creating a large-gradient preplasma and thus changing laser light absorption processes and electron-transport phenomena [15]. The prepulse was not measured during the experiment due to a technical problem, but measurements after the experiment indicate a prepulse intensity of $>10^{14}$ W/cm^2 over 3 ns.

V. SUMMARY AND OUTLOOK

In summary, we have presented the first radiography of a compressed iron sample with 60 keV x rays. Despite a low x-ray flux, probably originating from poor prepulse control during the experiment, it is possible to extract quantitative data due to an on-shot calibration of the line density. With the present x-ray flux, we cannot discriminate different EOS models, as the error is still too high. Considering the possible increase in photon flux, which can be achieved by improving the laser performance, as seen previously on other laser systems [8], a 1% precision for the line density can be expected. In this case, this method delivers much better compression data than conventional techniques based on shock and particle velocity measurements.

The successful demonstration of the on-shot calibration also opens the possibility of high-precision radiography with even higher photon energies, thus using continuum radiation above 100 keV. The technique can then be applied to larger samples or even high-Z materials.

The experiments also show the importance of a high laser contrast. Especially for high-energy laser systems this may require supplementary contrast improvement such as plasma mirrors, frequency doubling or nonlinear pulse cleaning [16].

ACKNOWLEDGMENTS

We thank the crew of the LULI 2000 laser system for their ongoing help during the experiment. This work was supported by the ANR project SECHEL, the Core-to-Core program from the JSPS, and the Global COE Program, "Center for Electronic Devices Innovation," from the Ministry of Education, Culture, Sports, Science and Technology of Japan. C.G. was supported by grants from the région Ile-de-France.

[1] B. A. Remington, R. P. Drake, and D. D. Ryutov, Rev. Mod. Phys. **78**, 755 (2006).
[2] J. Nguyen and N. Holmes, Nature (London) **427**, 339 (2004).
[3] J. D. Lindl, P. Amendt, R. L. Berger, S. G. Glendinning, S. H. Glenzer, S. W. Haan, R. L. Kauffman, O. L. Landen, and L. J. Suter, Phys. Plasmas **11**, 339 (2004).
[4] R. L. McCrory, D. D. Meyerhofer, R. Betti, R. S. Craxton, J. A. Delettrez, D. H. Edgell, V. Y. Glebov, V. N. Goncharov, D. R. Harding, D. W. Jacobs-Perkins, J. P. Knauer, F. J. Marshall, P. W. McKenty, P. B. Radha, S. P. Regan, T. C. Sangster, W. Seka, R. W. Short, S. Skupsky, V. A. Smalyuk, J. M. Soures, C. Stoeckl, B. Yaakobi, D. Shvarts, J. A. Frenje, C. K. Li, R. D. Petrasso, and F. H. Séguin, Phys. Plasmas **15**, 055503 (2008).
[5] A. Benuzzi-Mounaix, M. Koenig, G. Huser, B. Faral, D. Batani, E. Henry, M. Tomasini, B. Marchet, T. Hall, M. Boustie, T. De Resseguier, M. Hallouin, F. Guyot, D. Andrault, and T. Charpin, Phys. Plasmas **9**, 2466 (2002).
[6] H.-S. Park, D. M. Chambers, H.-K. Chung, R. J. Clarke, R. Eagleton, E. Giraldez, T. Goldsack, R. Heathcote, N. Izumi, M. H. Key, J. A. King, J. A. Koch, O. L. Landen, A. Nikroo, P. K. Patel, D. F. Price, B. A. Remington, H. F. Robey, R. A. Snavely, D. A. Steinman, R. B. Stephens, C. Stoeckl, M. Storm, M. Tabak, W. Theobald, R. P. J. Town, J. E. Wickersham, and B. B. Zhang, Phys. Plasmas **13**, 056309 (2006).
[7] H.-S. Park, B. R. Maddox, E. Giraldez, S. P. Hatchett, L. T. Hudson, N. Izumi, M. H. Key, S. L. Pape, A. J. MacKinnon, A. G. MacPhee, P. K. Patel, T. W. Phillips, B. A. Remington, J. F. Seely, R. Tommasini, R. Town, J. Workman, and E. Brambrink, Phys. Plasmas **15**, 072705 (2008).
[8] E. Brambrink, H. G. Wei, B. Barbrel, P. Audebert, A. Benuzzi-Mounaix, T. Boehly, T. Endo, C. Gregory, T. Kimura, R. Kodama, N. Ozaki, H.-S. Park, M. R. le Gloahec, and M. Koenig, Phys. Plasmas **16**, 033101 (2009).
[9] A. Ravasio, M. Koenig, S. L. Pape, A. Benuzzi-Mounaix, H. S. Park, C. Cecchetti, P. Patel, A. Schiavi, N. Ozaki, A. Mackinnon, B. Loupias, D. Batani, T. Boehly, M. Borghesi, R. Dezulian, E. Henry, M. Notley, S. Bandyopadhyay, R. Clarke, and T. Vinci, Phys. Plasmas **15**, 060701 (2008).
[10] M. Sonoda, M. Takano, J. Miyahara, and H. Kato, Radiology **148**, 833 (1983).
[11] L. Barker and R. E. Hollenbach, J. Appl. Phys. **41**, 4208 (1970).
[12] E. Brambrink, H. G. Wei, B. Barbrel, P. Audebert, A. Benuzzi, T. Boehly, T. Endo, C. Gregory, Tomoaki Kimura, R. Kodama, Norimasa Ozaki, H.-S. Park, Marc Rabec Le Gloahec, and M. Koenig (unpublished).
[13] R. Ramis, R. Schmalz, and J. Meyer-Ter-Vehn, Comput. Phys. Commun. **49**, 475 (1988).
[14] Sesame, The Lanl Equation of State Database, Los Alamos National Laboratories Technical Report No. LA-UR-92–3407, 1992 (unpublished).
[15] S. D. Baton, M. Koenig, J. Fuchs, A. Benuzzi-Mounaix, P. Guillou, B. Loupias, T. Vinci, L. Gremillet, C. Rousseaux, M. Drouin, E. Lefebvre, F. Dorchies, C. Fourment, J. J. Santos, D. Batani, A. Morace, R. Redaelli, M. Nakatsutsumi, R. Kodama, A. Nishida, N. Ozaki, T. Norimatsu, Y. Aglitskiy, S. Atzeni, and A. Schiavi, Phys. Plasmas **15**, 042706 (2008).
[16] A. Jullien, O. Albert, F. Burgy, G. Hamoniaux, L. Rousseau, J. Chambaret, F. Auge-Rochereau, G. Cheriaux, J. Etchepare, N. Minkovski, and S. Saltiel, Opt. Lett. **30**, 920 (2005).